JACS Au
AN OPEN ACCESS JOURNAL OF THE AMERICAN CHEMICAL SOCIETY

pubs.acs.org/jacsau
Article

Versatile Split-and-Mix Liposome PROTAC Platform for Efficient Degradation of Target Protein *In Vivo*

Chunli Song,‖ Zijun Jiao,‖ Zhanfeng Hou,‖ Yun Xing, Xinrui Sha, Yuechen Wang, Jiaxin Chen, Susheng Liu, Zigang Li,* and Feng Yin*

Cite This: *JACS Au* 2024, 4, 2915−2924
Read Online

ACCESS | Metrics & More | Article Recommendations | Supporting Information

ABSTRACT: PROTAC (Proteolysis TArgeting Chimeras) is a promising therapeutic approach for targeted protein degradation that recruits an E3 ubiquitin ligase to a specific protein of interest (POI), leading to its degradation by the proteasome. Recently, we developed a novel split-and-mix PROTAC system based on liposome self-assembly (LipoSM-PROTAC) which could achieve target protein degradation at comparable concentrations comparable to small molecules. In this study, we expanded protein targets based on the LipoSM-PROTAC platform and further examined its therapeutic effects *in vivo*. Notably, this platform could efficiently degrade the protein level of MEK1/2 in A375 cells or Alk in NCI-H2228 cells and display obvious tumor inhibition (60−70% inhibition rate) with negligible toxicity. This study further proved the LipoSM-PROTAC's application potentials.

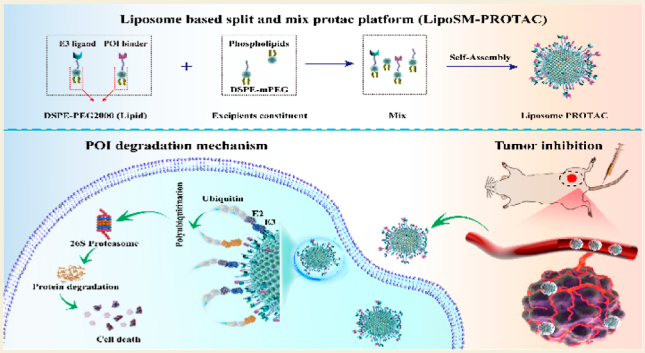

KEYWORDS: *split-and-mix, LipoSM-PROTAC, protein degradation, in vivo therapeutic, tumor inhibition*

INTRODUCTION

The field of targeted protein degradation has attracted significant interest in recent years, which offers a promising approach to the development of new therapeutics for a range of diseases.[1−4] Since ARV-110 and ARV-471 went into phase-II clinical trials, a research boom for PROTAC appeared in the biopharmaceutical industry, promoting the innovation and progression of PROTAC technology.[5,6] The advantages of PROTAC technology lay in its ability to overcome the nondruggability and suppress the resistant mutation by directing specific proteins to the ubiquitin−proteasome protein degradation machinery.[7−10] These advantages could propel drug development and provide novel approaches for personalized and precision medicine.[11] Yet, some challenges still exist, such as poor membrane penetration and time-consuming drug screening, etc., which have further limited the clinical applications of traditional PROTAC.[6,12,13] To address these challenges, our group designed a novel peptide-based self-assembly PROTAC nanoplatform (SM-PROTAC) with facile screening, programmable ligand ratios, self-optimized biomolecule spatial recognition, and multifunctional properties that hold great promise as a targeted protein degradation strategy.[14] However, this peptide-based SM-PROTAC platform requires high dosing (50−100 μM) for effective protein of interest (POI) degradation. Recently, we reported a novel LipoSM-PROTAC platform that could selectively degrade POI and address the low efficiency of the SM-PROTAC platform.[15] However, only cellular level study was performed, and more detailed study, such as the *in vivo* efficacy and safety evaluation, is highly desirable to further support this system's possible further application. In this study, we expanded protein targets based on the LipoSM-PROTAC platform and further examined its therapeutic effects *in vivo*.

MEK and Alk are considered potent oncogenic drivers in cancer and other diseases.[16−19] The MEK and Alk inhibitors' development is a focused area for drug development.[19,20] Herein, we develop a new PROTAC based on the LipoSM system to degrade the protein levels of MEK or ALK at single digit micromolar concentration at the cellar level. Then, the *in vivo* therapeutic efficacy was examined for MEK, which showed higher efficiency than its small molecule counterpart (20 mg/kg vs 50 mg/kg, one dose/2 days vs one dose/per day).[21]

First, we successfully prepared liposome particles with uniform sizes by utilizing the synthesized DSPE-PEG2000-E3 recruiters, DSPE-PEG2000-POI recruiters, and liposome excipients as effective ingredients. Second, the POI recruiters and E3 recruiters were distributed on the surface of liposome

Received: March 28, 2024
Revised: June 15, 2024
Accepted: June 17, 2024
Published: July 11, 2024

Scheme 1. Illustration of the Targeted Protein Degradation for Inhibition Tumor Proliferation Nanoplatforms Based on Split-and-Mix Liposome PROTAC

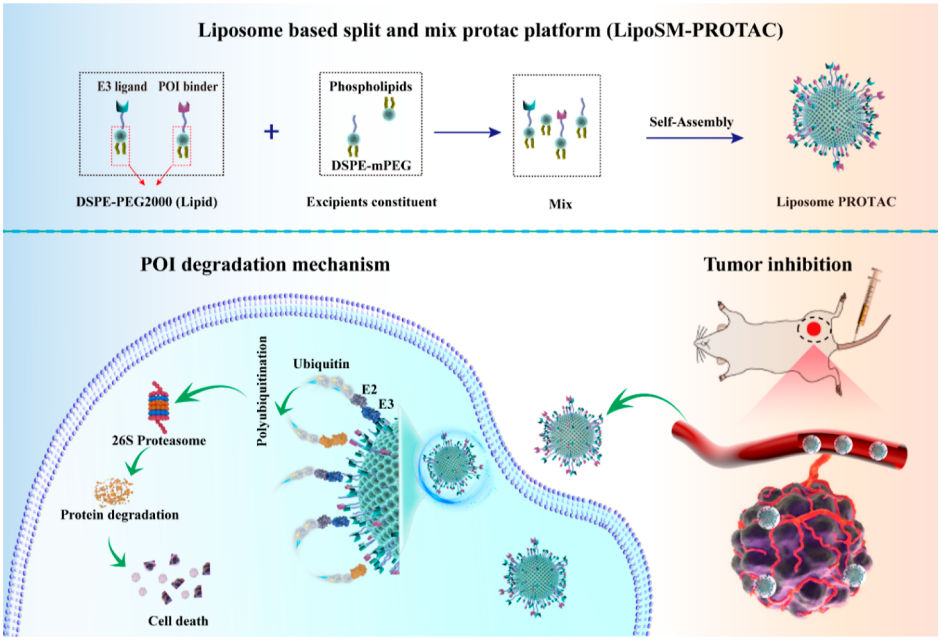

nanospheres in a regulated ligand ratio, facilitating the proximity of intramolecular or intermolecular E3 ligases to the POI. This proximity promoted the degradation of POI by the endogenous 26S proteasome on a spatial scale.[22] In this study, we incorporated MEK and Alk as model targets to assess the efficacy of the LipoSM-PROTAC platform. The results demonstrated that our platform has exceptional therapeutic efficacy (60−70% inhibition rate) and biological safety *in vivo* for MEK targets (Scheme 1). Together, LipoSM-PROTAC presented unique advantages such as good biocompatibility and significant potential for clinical translation. We anticipate that this LipoSM-PROTAC system with the flexibility reported in this work will provide reference strategies for gene therapy, cell therapy, and immunotherapy.

RESULTS AND DISCUSSION

Synthesis and Characterization of DSPE-PEG2000 Conjugates

First, to further broaden the applications of the LipoSM-PROTAC platform, the novel MEK1/2 and Alk degraders were designed, composed of a MEK1/2 or Alk binding module and a von Hippel−Lindau (VHL) E3 ligase-recruiting element, which can regulate the intracellular ubiquitin−proteasome system to degrade target proteins. In this system, the functional group NHS of DSPE−PEG−NHS was selected as the reactive group, which could react with the amino functional groups of the VHL, Mitb (mirdametinib analogue), and Cetb (ceritinib) to modify the small-molecule drug by PEGylation (Figure 1A−C). Next, the structures of DSPE-PEG2000-VHL, DSPE-PEG2000-Mitb, and DSPE-PEG2000-Cetb were characterized by using high-resolution mass spectrometry (HRMS) (Figure S1). According to the HRMS spectrum, the average molecular weight distribution of the DSPE-PEG2000-NHS was about 3000, but the DSPE-PEG2000-VHL, DSPE-PEG2000-Mitb, and DSPE-PEG2000-Cetb were increased to about 3500 after the reaction. These data analyses confirmed that DSPE-PEG2000 conjugates could be successfully synthesized with a simple approach.

Preparation and Characterization of Liposomes

First, the thin-film hydration and extrusion method was used to prepare the liposomes. As shown in Figure 1D,E, the particle sizes of prepared Excip (without DSPE-PEG2000-VHL and DSPE-PEG2000-Mitb), V-L (DSPE-PEG2000-VHL liposome), Mitb-L (DSPE-PEG2000-Mitb liposome), and V-Mitb-L (DSPE- PEG2000-VHL and DSPE-PEG2000-Mitb liposome) were about 150 nm with a narrow polydispersity index (<0.3). Dynamic light scattering (DLS) measurements indicated that these particles had a negative surface charge (Figure 1F). We then tested the stability of Excip, V-L, Mitb-L, and V-Mitb-L in DMEM medium, phosphate-buffered saline (PBS), and 1640 medium and found that all particle sizes were nearly unchanged after 48 h storage at 4 °C (Figures 1G, S2A, and S2B), indicating satisfactory stability of the particles under physiological environmental condition. The morphology of as-prepared V-L, Mitb-L, and V-Mitb-L was tested by scanning electron microscopy (SEM) as shown in Figure 1H, where the particles were displayed as uniform and spherical with distinct outlines. Moreover, the SEM−EDX element mapping revealed that a single nanosphere of V-L and Mitb-L contained S and F elements, respectively, and the V-Mitb-L nanosphere simultaneously contained S and F elements, indicating that DSPE-PEG2000-VHL and DSPE-PEG2000-Mitb were successfully modified onto the V-Mitb-L nanosphere (Figure S3). These results demonstrated the successful assembly of these liposome particles.

Cellular Distribution and Uptake of Liposomes

To investigate the drug distribution and uptake efficiency of liposomes on a cellular level, the DSPE-PEG2000 copolymer was labeled with the fluorescent dye FITC and Cy5 instead of VHL and Mitb to observe liposome drugs' intracellular distributions (Figure S4A). The flow cytometry analysis indicated that fluorescence signals gradually increased as the

https://doi.org/10.1021/jacsau.4c00278
JACS Au 2024, 4, 2915−2924

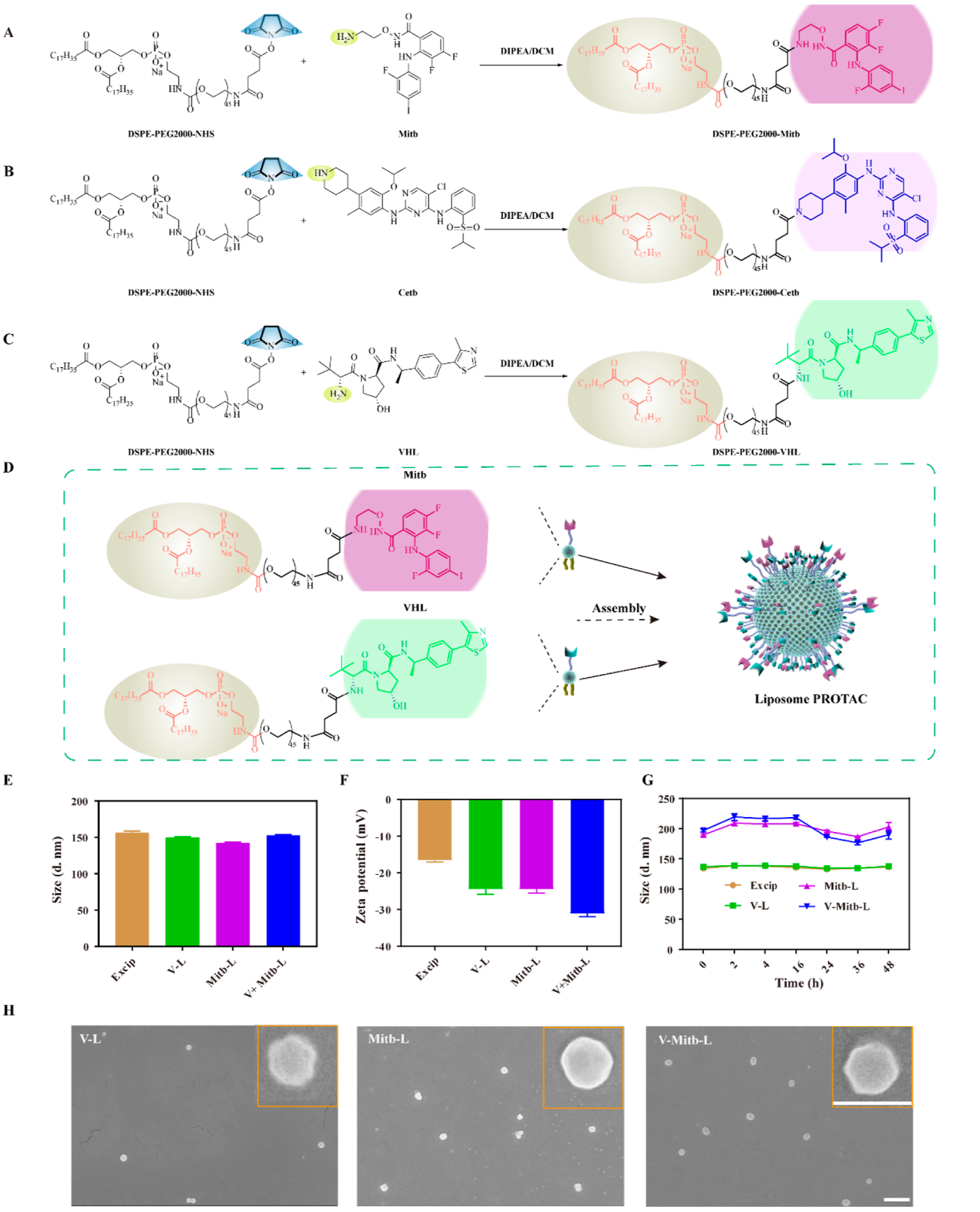

Figure 1. Synthesis route of (A) DSPE-PEG2000-Mitb, (B) DSPE-PEG2000-Cetb, and (C) DEPE-PEG2000-VHL. (D) Chemical structure of DSPE-PEG2000-Mitb (POI recruitment module) and DSPE-PEG2000-VHL (VHL, E3 ligase recruitment module). (E) Particle size distribution of Excip, V-L, Mitb-L, and V-Mitb-L measured via DLS. (F) Zeta potential distribution of Excip, V-L, Mitb-L, and V-Mitb-L. (G) Stability of Excip, V-L, Mitb-L, and V-Mitb-L in DMEM (5% FBS) measured by sizes via DLS. (H) SEM images of particles. Scale bar = 1 μm and enlarged scale bar = 200 nm. Error bars represent SEMs of at least three independent measurements.

incubation time was extended (Figure S4B,C). The confocal microscopic imaging showed that two fluorescence signals remarkably increased as the incubation time extended, and two fluorescent signals were colocalized well (Pearson's correlation

https://doi.org/10.1021/jacsau.4c00278
JACS Au 2024, 4, 2915−2924

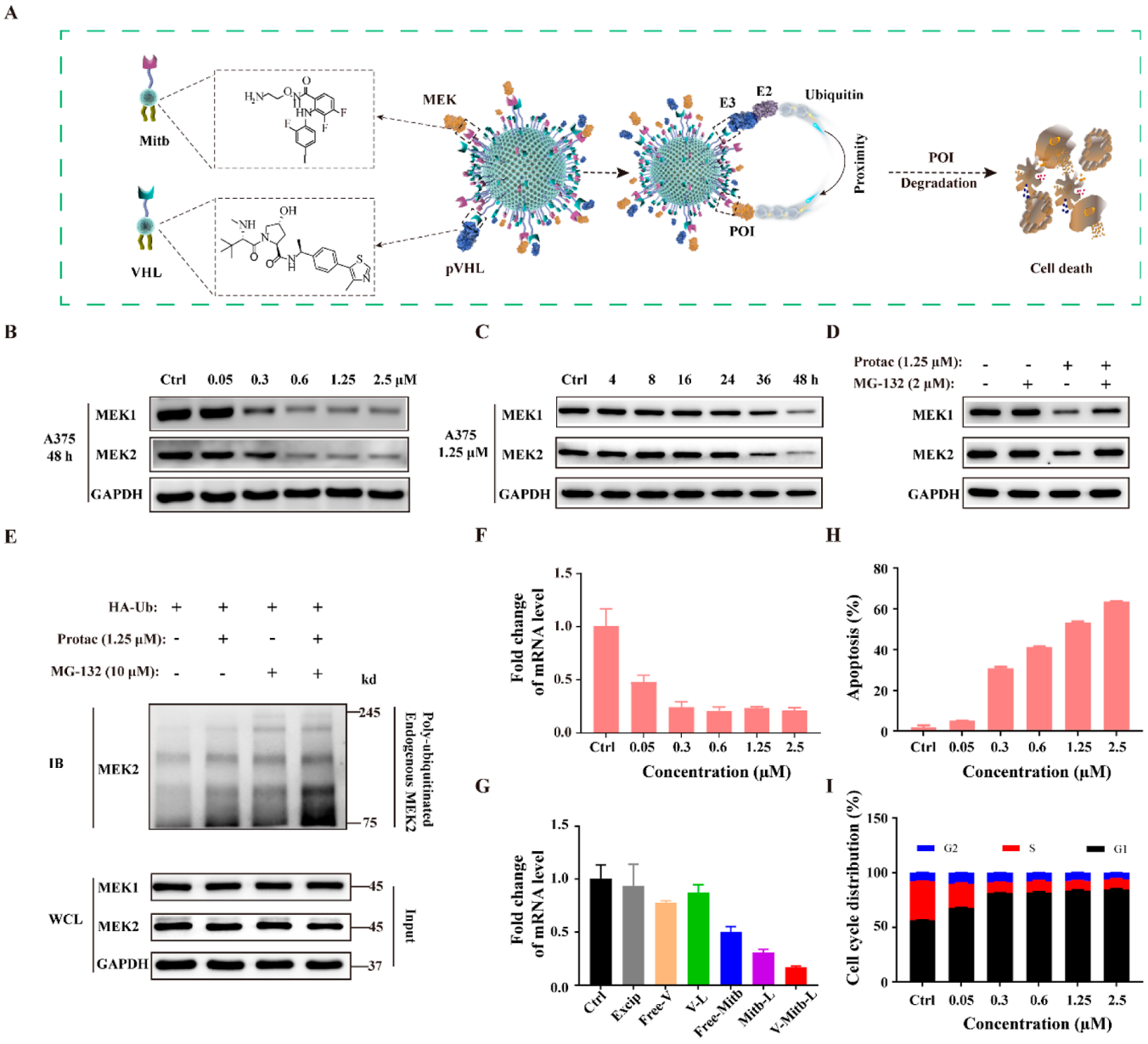

Figure 2. (A) Schematic diagram of MEK1/2 degrader-based degradation model via the proteasome. (B) WB analysis of the MEK1/2 degradation in A375 cells treated with different doses of V-Mitb-L for 48 h. (C) WB analysis of the MEK1/2 degradation of A375 cells treated with 1.25 μM V-Mitb-L at different time points (4, 8, 16, 24, 36, and 48 h). (D) MEK1/2 levels in A375 cells after being treated with 1.25 μM V-Mitb-L (with or without 2 μM MG132) for 48 h. (E) Immunoprecipitation-WB analysis of the ubiquitinated MEK2 levels in A375 cells after treating with 1.25 μM V-Mitb-L (with or without 10 μM MG132) for 8 h. (F) Expression levels of endogenous MEK-related genes Klf4 in A375 cells after treating with different doses of V-Mitb-L (0.05, 0.3, 0.6, 1.25, and 2.5 μM) for 24 h (normalized to the mRNA levels of GAPDH). (G) Expression levels of endogenous MEK-related genes Klf4 in A375 cells after treatment with different nanoformulations for 24 h. (H) Apoptosis of A375 cells was quantitatively analyzed by Annexin V/PI staining after treatment with different doses of V-Mitb-L (0.05, 0.3, 0.6, 1.25, and 2.5 μM). (I) The cycle of the A375 cells was quantitatively analyzed by PI staining combined with flow cyto-fluorometry after treatment with different doses of V-Mitb-L (0.1, 0.6, 1.25, and 2.5 μM). Error bars represent SEMs of at least three independent measurements.

coefficient, R = 0.85) (Figure S4D−G). The results demonstrated that the two modules remained in one nanosphere after cellular uptake. Taken together, these data illustrated that liposomes could efficiently transport drugs into the cells.

Evaluation of the Degradation Activity *In Vitro*

Mitb is an inhibitor of MEK (MEK1/MEK2), which shows obvious tumor inhibition *in vivo*.[23] In this study, the MEK LipoSM-PROTAC (V-Mitb-L) was developed with a Mitb recruit module and a VHL ubiquitin ligase-recruit module. Since VHL is a tumor suppressor, resistance mechanisms in VHL-based PROTACs are primarily due to alterations or mutations in the E3 ligase genome. Additionally, different types of E3 ligases exhibit varying expression levels in different cell types, leading to differences in the degradation activity and efficiency. Different target proteins also exhibit varying selectivity toward E3 ligases, resulting in varying E3 ligase-induced protein ubiquitination and degradation efficiency. Furthermore, some proteins have greater tolerance to E3 ligases, allowing researchers to utilize multiple E3 ligases (such

https://doi.org/10.1021/jacsau.4c00278
JACS Au 2024, 4, 2915−2924

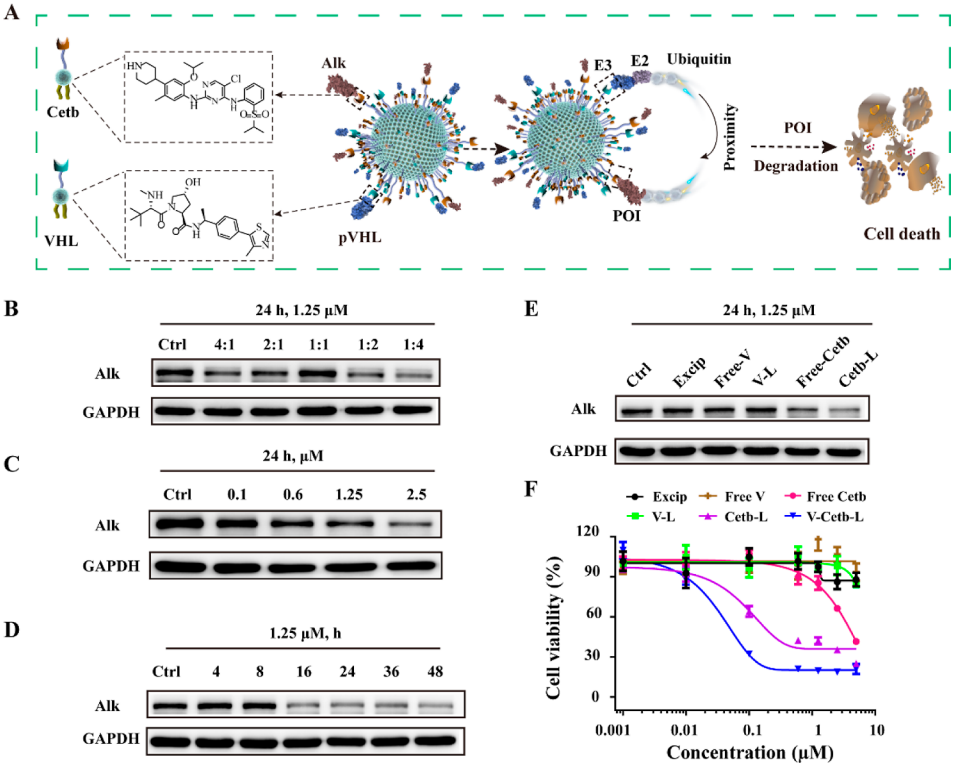

Figure 3. (A) Schematic diagram of the Alk degrader-based degradation model via the proteasome. (B) WB analysis of the Alk degradation in NCI-H2228 cells treated with 1.25 μM V-Cetb-L with different molar ratios (4:1−1:4) for 24 h. (C) WB analysis of the Alk degradation in NCI-H2228 cells treated with different doses of V-Cetb-L for 24 h. (D) WB analysis of the Alk degradation in NCI-H2228 cells treated with 1.25 μM V-Cetb-L at different time points (4, 8, 16, 24, 36, and 48 h). (E) WB analysis of the Alk degradation in NCI-H2228 cells treated with different formulations. (F) Cell viability of NCI-H2228 cells treated with different doses of Excip (excipients, without drug), V-L (VHL-liposome), free V (free VHL), Cetb-L (ceritinib-liposome), free Cetb (free ceritinib), and V-Cetb-L (VHL-ceritinib-liposome) for 24 h. Error bars represent SEMs of at least three independent measurements.

as CRBN, VHL, MDM2, and cIAP) in the design of PROTACs. The split-and-mix liposome PROTAC system, designed to target various proteins for degradation using different E3 ligases, is currently undergoing verification. Here, we primarily investigate the PROTACs based on VHL in degrading MEK1/2 or Alk.

The western blot (WB) analysis was conducted to assess the ability of the V-Mitb-L degrader to induce the degradation of mitogen-activated protein kinase (MEK1/MEK2) in A375 cells (Figure 2A). The WB results clearly showed that the group with a ratio of 1:4 had the best degradation effect on MEK (Figure S5A); hence, all following *in vitro* inhibition experiments were implemented with this ratio. Next, the WB results further revealed that the MEK protein could be degraded in dose- and time-dependent manners (Figures 2B,C and S5B). Compared with other groups, MEK was significantly degraded in the V-Mitb-L group, which suggested that LipoSM-PROTAC-mediated protein degradation was dependent on the E3 and POI moieties (Figures 2B and S5B).

To investigate the MEK protein degradation pathway, the A375 cells were treated with V-Mitb-L in the presence or absence of proteasome inhibitor MG132 and E1 ubiquitin-activating enzyme inhibitor MLN7243 (Figures 2D,E, S6A, and S6B). The results suggested that the V-Mitb-L could efficiently degrade MEK through a ubiquitin−proteasome-dependent pathway. Furthermore, we verified whether a free VHL ligand could efficiently block V-Mitb-L in degrading MEK1/2 (Figure S6C). The results showed that the VHL ligand could efficiently block V-Mitb-L in degrading MEK1/2 after stimulating A375 cells.

Research has shown that Klf4 was an MEK target in some melanoma cell lines.[24,25] Here, we used quantitative polymerase chain reaction (qPCR) analysis to further test the mRNA levels of the downstream gene Klf4, which was transcriptionally regulated by MEK. As shown in Figure 2F,G, A375 cells treated with V-Mitb-L resulted in a significant decrease in the mRNA levels of the Klf4 gene in a concentration-dependent manner. Besides, the V-Mitb-L group had a significant effect on Klf4 gene expression in all formulations.

Effects of Liposome on Cell Proliferation

We next evaluated whether the liposomes could inhibit the A375 cell proliferation. Cell Counting Kit-8 assay was conducted on A375 cells to evaluate the cytotoxicity of the liposomes. The result showed that the V-Mitb-L group exhibited significant suppression in cell proliferation in a dose-dependent manner, with an IC50 of 0.046 μM (Figures S7 and S8), which further revealed that V-Mitb-L was effective at inhibiting proliferation in A375 cells. Moreover, we assessed the cell apoptosis and cell cycle distribution induced by V-Mitb-L in A375 cells using flow cytometry analysis (Figures 2H and S9A,B). As expected, the V-Mitb-L-induced apoptosis appeared to be in a concentration-dependent manner, and the drug-induced apoptotic rate reached 62% (early and advanced apoptosis). Additionally, we simultaneously investigated whether the V-Mitb-L drugs could have an effect on cell cycle distribution in A375 cells, and the data further confirmed

https://doi.org/10.1021/jacsau.4c00278
JACS Au 2024, 4, 2915−2924

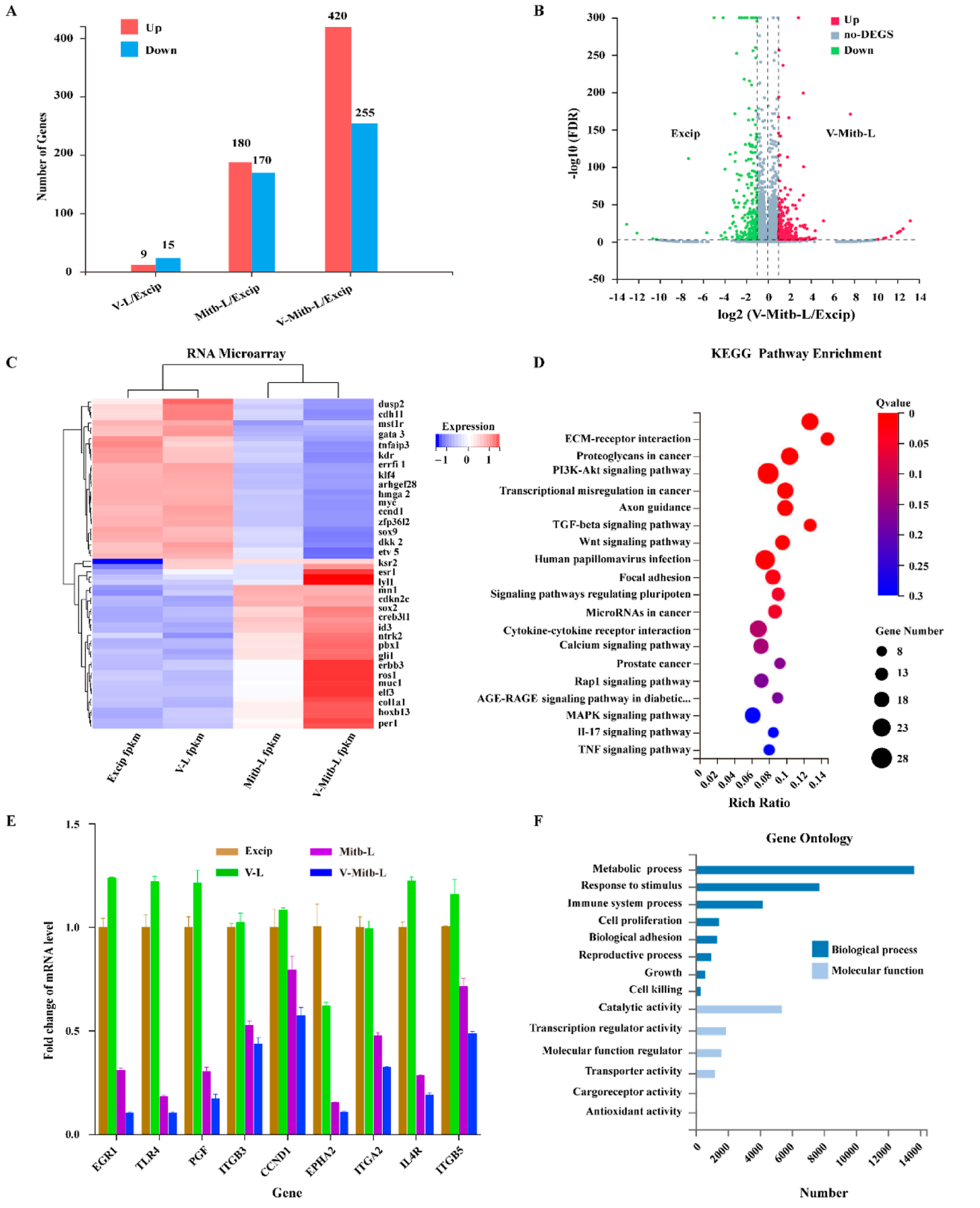

Figure 4. (A) Microarray analysis of upregulated and downregulated genes in A375 cells treated with V-L, Mitb-L, and V-Mitb-L, compared to the Excip group. (B) Differential expression of genes between V-Mitb-L and Excip groups. The upregulated, downregulated, and unchanged genes were dotted in red, green, and gray, respectively. (C) Heat map of differentially expressed genes in RNA-microarray analysis performed on Excip-, V-L-, Mitb-L-, and V-Mitb-L-treated A375 cells. (D) KEGG analysis revealed different signaling pathways influenced by V-Mitb-L treatment in A375 cells, compared to the Excip treatment group. (E) Changes in the expression of the EGR1, TLR4, PGF, ITGB3, CCND1, EPHA2, ITGA2, IL4R, and ITGB5 genes in Excip-, V-L-, Mitb-L-, and V-Mitb-L-treated A375 cells. (F) Enriched gene ontology analysis influenced by V-Mitb-L in A375 cells compared to the Excip group. Error bars represent SEMs of at least three independent measurements.

https://doi.org/10.1021/jacsau.4c00278
JACS Au 2024, 4, 2915−2924

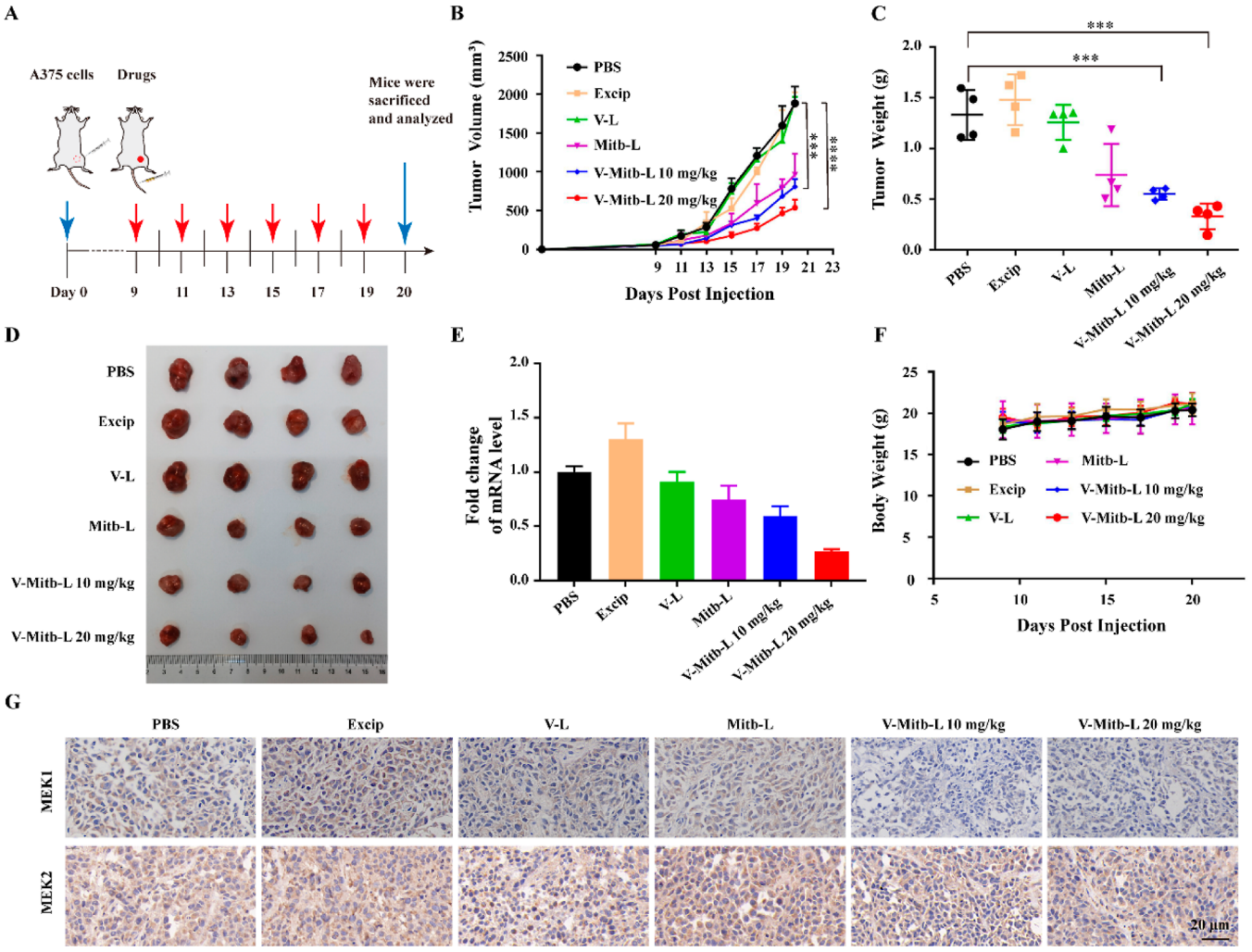

Figure 5. (A) Administration plans for BALB/c mice. After subcutaneous injection of A375 cells (2×10^6), mice were treated with the indicated formulations every 2 days. (B) Average A375 tumor growth curve ($n = 4$). (C,D) A375 tumor weight statistics and tumor tissue dissected images of mice after treatment. (E) Expression levels of MEK-related genes Klf4 in tumor tissues after treatment. (F) Average body growth curves of mice throughout treatment. (G) Immunohistochemistry-stained sections of the tumor tissues after treatment. Data are presented as mean ± SEM ($n = 3$). Data are analyzed by one-way ANOVA (*$p < 0.05$, **$p < 0.01$, ***$p < 0.001$).

that the A375 cells were arrested in the G1 phase compared to the untreated group (Figures 2I and S9C). These results suggested that our as-prepared V-Mitb-L can efficiently induce A375 cell apoptosis and influence the cell cycle distribution.

Bioactivity Evaluation of Other Targets *In Vitro*

Furthermore, to verify the generality of the LipoSM-PROTAC system, the DSPE-PEG2000-Cetb polymer was utilized to construct V-Cetb-L LipoSM-PROTAC for Alk degradation (Figure 3A). As shown in Figure S10A,B, the V-Cetb-L particles were successfully prepared, which proved the versatility of our method. The WB experiment clearly showed that the ratio of the 1:4 (VHL: Cetb) group had the best degradation effect on Alk (Figure 3B). Therefore, all *in vitro* experiments were performed at this ratio. Furthermore, WB results revealed that the degradation of Alk in NCI-H2228 cells was both dose and time dependent (Figure 3C,D). Moreover, as shown in Figure 3E,F, the V-Cetb-L-treated NCI-H2228 cells displayed the best inhibition efficiency and degradation effectiveness among all treated groups. Besides, we verified whether the free VHL ligand could efficiently block V-Cetb-L in degrading Alk (Figure S11). The results showed that the VHL ligand could efficiently block V-Cetb-L in degrading Alk after stimulating NCI-H2228 cells. In summary, these results were consistent with the *in vitro* degradation results of MEK, demonstrating that our LipoSM-PROTAC system could be utilized as a general platform for the degradation of multiple targets.

Transcriptome Analysis *In Vitro*

To explore the effect of LipoSM-PROTAC on different signal pathways, we utilized an RNA transcriptome approach for the in-depth analysis of the associated gene expression. The grouped samples revealed a good correlation via the Pearson correlation coefficient analysis (Excip similarly V-L, Mitb-L similarly V-Mitb-L) (Figure S12).[26] As shown in Figures 4A,B and S13, the A375 cells treated with the V-L and Mitb-L displayed 9 and 180 upregulated and 15 and 170 down-regulated genes, respectively; whereas, the V-Mitb-L treatment demonstrated 420 upregulated and 255 downregulated genes, indicating different gene expression patterns. We then evaluated the gene profiles between the Excip and different groups via the heat-map analysis, and the results were

https://doi.org/10.1021/jacsau.4c00278
JACS Au 2024, 4, 2915−2924

consistent with the volcano plot where the V-Mitb-L showed obvious differences (Figure 4C).

Signaling pathways, including PI3K-Akt, Wnt, MAPK, etc., were reported to regulate cell proliferation, differentiation, and apoptosis.[27−29] Here, we focused on exploring whether the signaling pathway showed remarkable changes after being treated with V-Mitb-L in A375 cells. Kyoto Encyclopedia of Genes and Genomes (KEGG) functional enrichment analysis revealed that more than 20 important signaling pathways such as PI3K-Akt, Wnt, MAPK, etc., were affected by V-Mitb-L drugs (Figure 4D). Therefore, several downregulated genes, such as EGR1, TLR4, PGF, ITGB3, CCND1, EPHA2, ITGA2, IL4R, and ITGB5 genes in the PI3K-Akt signaling pathway, were selected as candidates to verify the changes in their mRNA expressions by RT-qPCR. The RT-qPCR results were consistent with the KEGG analysis, demonstrating that the V-Mitb-L group repressed the gene expressions of these candidates compared to other treatment groups (Figure 4E). Additionally, we further performed gene ontology analysis on the functions of the differentially expressed genes. The result indicated that these genes mainly affected biological processes and molecular function (Figure 4F). Many researchers have shown that these biological processes are closely associated with certain genes in metabolic pathways, such as the growth factor receptor (EGFR), Krüppel-like factor 4 (KLF4), and peroxisome proliferator-activated receptor gamma (PPARG). In this study, genes like EGFR, PPARG, and KLF4 exhibit significant differences. The EGFR family signaling pathway activates the RAS/RAF/MEK/ERK pathway for cell cycle progression and DNA synthesis and the PI3K/AKT/mTOR pathway for protein synthesis and metabolism, playing a crucial role in metabolic processes.[30] Investigators reported that KLF4 can interact with β-catenin, influencing the Wnt signaling pathway essential for cell proliferation, differentiation, and metabolic development.[31] Additionally, PPARG can modulate the inflammatory response by inhibiting the production of inflammatory factors, such as those mediated by the NF-κB pathway.[32] Therefore, these findings suggest that V-Mitb-L could potentially impact the expression of various signaling pathways. Specifically, V-Mitb-L might influence the EGFR pathway, thereby affecting cell cycle and metabolic regulation, altering the interaction of KLF4 with β-catenin to modify Wnt signaling and regulate PPARG activity to modulate inflammatory responses. Consequently, by modulation of these critical signaling pathways, the LipoSM-PROTAC platform could emerge as a significant regulator in cancer therapies.

Evaluation of the Antitumor Activity *In Vivo*

Encouraged by the high degradation efficiency of LipoSM-PROTAC for MEK *in vitro*, we subsequently evaluated the therapeutic effects against tumors *in vivo* by establishing a subcutaneous xenograft A375 melanoma tumor-bearing mice model. The tumor-bearing mice were administered with PBS, Excip, V-L, Mitb-L, and V-Mitb-L by tail vein injection at a dosage of 10.0 mg/kg for V-Mitb-L, 20 mg/kg for other groups, every 2 days for 6 treatments (Figure 5A). As shown in Figure 5B (tumor volume), 5C (tumor weight), and 5D (tumor image), the group of mice treated with 20 mg/kg V-Mitb-L produced a more distinct tumor growth suppression effect than the 10 mg/kg V-Mitb-L group. As with our rational design, the 20 mg/kg V-Mitb-L group exhibited the best antitumor effect compared to all of the control groups *in vivo*. After the indicated treatments, we performed quantitative real-time PCR (qPCR) analysis to validate the gene expression levels in tumor tissues. The gene expression analysis indicated significant downregulation of the Klf4 gene after treatment with 20 mg/kg V-Mitb-L (Figure 5E). Besides, immunofluorescence experiments revealed that the fluorescence intensity of the MEK protein was the weakest in the tumor tissue of 20 mg/kg of V-Mitb-L-treated mice, suggesting the potential suppression of MEK protein expression *in vivo* (Figure 5G). Mitb showed favorable therapeutic effects with oral administration with a dosage of 50 mg/kg/per day, and our LipoSM-PROTAC showed similar antitumor activity *in vivo* with 20 mg/kg and one dose/two day.[21] These results suggested that the LipoSM-PROTAC system has comparable efficacy as its small molecule counterpart.

Finally, we further examined the effects of treatments on body weight to assess their possible systemic toxicity. During the treatment, we observed that the body weight of mice did not change significantly (Figure 5F), indicating the excellent biosafety of this LipoSM-PROTAC system. Meanwhile, the hemolysis experiment also proved the excellent hemocompatibility of this system (Figure S14). Moreover, the tissue of major organs (heart, liver, spleen, lung, kidney, and brain) was used to evaluate the general toxicity of these formulations using hematoxylin and eosin (H&E) staining (Figure S15). Compared to the PBS control, none of the experimental groups displayed notable morphological differences in H&E staining. Taken together, our *in vivo* experiments confirmed that the LipoSM-PROTAC system could be a promising nano platform for clinical applications of cancer therapy.

CONCLUSIONS

The design and the optimization of PROTAC molecules required significant expertise and resources, as it could be challenging and time-consuming to achieve the right balance of target binding affinity, cellular permeability, and proteasome degradation efficiency.[33] In our previous study, we successfully developed a peptide-based SM-PROTAC system and further evolved it into a more efficient liposome-based SM-PROTAC. In this study, we expanded other targets based on the LipoSM-PROTAC platform and carefully evaluated its *in vivo* efficiency and safety. The results suggested that this platform could efficiently degrade the protein level of MEK in A375 cells or Alk in NCI-H2228 cells, along with obvious tumor inhibition (60−70% inhibition rate) and negligible toxicity. These results further validated the LipoSM-PROTAC's biocompatibility and its potential for clinical translation, offering the capability for multiple POI targeting and other chimera-type applications. We anticipate that the LipoSM-PROTAC system presented in this work will provide huge potential in clinical applications, where its therapeutic area extends far beyond oncology.

ASSOCIATED CONTENT

Supporting Information

The Supporting Information is available free of charge at https://pubs.acs.org/doi/10.1021/jacsau.4c00278.

Compound synthesis, DLS analysis, SEM images, flow cytometric analysis, confocal analysis, WB analysis, cck8 assays, cell apoptosis analysis, cell cycle analysis, volcano plot analysis, hemolysis assays, H&E staining analysis, primers for RT-PCR analysis, and HRMS (PDF)

https://doi.org/10.1021/jacsau.4c00278
JACS Au 2024, 4, 2915−2924

AUTHOR INFORMATION

Corresponding Authors

Zigang Li − *State Key Laboratory of Chemical Oncogenomics, School of Chemical Biology and Biotechnology, Peking University Shenzhen Graduate School, Shenzhen 518055, China; Pingshan Translational Medicine Center, Shenzhen Bay Laboratory, Shenzhen 518118, China;* orcid.org/0000-0002-3630-8520; Email: lizg@pkusz.edu.cn

Feng Yin − *State Key Laboratory of Chemical Oncogenomics, School of Chemical Biology and Biotechnology, Peking University Shenzhen Graduate School, Shenzhen 518055, China; Pingshan Translational Medicine Center, Shenzhen Bay Laboratory, Shenzhen 518118, China*; Email: yinfeng@pkusz.edu.cn

Authors

Chunli Song − *State Key Laboratory of Chemical Oncogenomics, School of Chemical Biology and Biotechnology, Peking University Shenzhen Graduate School, Shenzhen 518055, China*

Zijun Jiao − *Pingshan Translational Medicine Center, Shenzhen Bay Laboratory, Shenzhen 518118, China; Frontiers Medical Center, Tianfu Jincheng Laboratory, Chengdu, Sichuan 610212, China*

Zhanfeng Hou − *State Key Laboratory of Chemical Oncogenomics, School of Chemical Biology and Biotechnology, Peking University Shenzhen Graduate School, Shenzhen 518055, China*

Yun Xing − *State Key Laboratory of Chemical Oncogenomics, School of Chemical Biology and Biotechnology, Peking University Shenzhen Graduate School, Shenzhen 518055, China*

Xinrui Sha − *Pingshan Translational Medicine Center, Shenzhen Bay Laboratory, Shenzhen 518118, China*

Yuechen Wang − *State Key Laboratory of Chemical Oncogenomics, School of Chemical Biology and Biotechnology, Peking University Shenzhen Graduate School, Shenzhen 518055, China*

Jiaxin Chen − *Pingshan Translational Medicine Center, Shenzhen Bay Laboratory, Shenzhen 518118, China*

Susheng Liu − *Pingshan Translational Medicine Center, Shenzhen Bay Laboratory, Shenzhen 518118, China*

Complete contact information is available at: https://pubs.acs.org/10.1021/jacsau.4c00278

Author Contributions

‖C.S., Z.J., and Z.H. have contributed equally to this work. Z.L. and F.Y. conceived the project. C.S. and J.Z. designed and performed all experiments. Z.H. performed material preparation and characterization. C.S., Z. J., X.S., and S.L. evaluated antitumor activity *in vitro* and *in vivo*. Y.W. measured the morphology of samples. J.C. analyzed RNA data. C.S. wrote the original draft and edited the manuscript. Y.X., Z.L., and F.Y. reviewed and edited the manuscript.

Notes

The authors declare no competing financial interest.

ACKNOWLEDGMENTS

This work was funded by the National Key R&D Program of China, 2021YFC2103900; Natural Science Foundation of China (grant no. 21977010); National Center for Biological Medicine Technology Innovation, NCTIB2022HS01017; Natural Science Foundation of Guangdong Province, 2022A1515010996; Shenzhen Science and Technology Program, RCJC20200714114433053; High-tech Zone Development Special Project of Shenzhen, 29853M-KCJ-2023-002-07; Tian Fu Jin Cheng Laboratory (Advanced Medical Center) Group Racing Project, TFJC2023010008; and Shenzhen-Hong Kong Institute of Brain Science-Shenzhen Fundamental Research Institutions, 2023SHIBS0004. This work was supported by the Proteomic Platform of Pingshan Translational Medicine Center, Shenzhen Bay Laboratory.

REFERENCES

(1) Wang, D.; Wang, W.; Fang, L.; Qi, L.; Zhang, Y.; Liu, J.; Liang, Y.; Yang, H.; Wang, M.; Wei, X.; Jiang, R.; Liu, Y.; Zhou, W.; Fang, X. Mitochondrial Protease Targeting Chimeras for Mitochondrial Matrix Protein Degradation. *J. Am. Chem. Soc.* **2023**, *145*, 12861−12869.

(2) He, M.; Cao, C.; Ni, Z.; Liu, Y.; Song, P.; Hao, S.; He, Y.; Sun, X.; Rao, Y. PROTACs: Great Opportunities for Academia and Industry (An Update from 2020 to 2021). *Signal Transduction Targeted Ther.* **2022**, *7*, 181.

(3) Khan, S.; He, Y.; Zhang, X.; Yuan, Y.; Pu, S.; Kong, Q.; Zheng, G.; Zhou, D. Proteolysis TArgeting Chimeras (PROTACs) as Emerging Anticancer Therapeutics. *Oncogene* **2020**, *39*, 4909−4924.

(4) Schneider, M.; Radoux, C. J.; Hercules, A.; Ochoa, D.; Dunham, I.; Zalmas, L. P.; Hessler, G.; Ruf, S.; Shanmugasundaram, V.; Hann, M. M.; Thomas, P. J.; Queisser, M. A.; Benowitz, A. B.; Brown, K.; Leach, A. R. The PROTACtable Genome. *Nat. Rev. Drug Discovery* **2021**, *20*, 789−797.

(5) Bekes, M.; Langley, D. R.; Crews, C. M. PROTAC Targeted Protein Degraders: the Past Is Prologue. *Nat. Rev. Drug Discovery* **2022**, *21*, 181−200.

(6) Li, X.; Song, Y. Proteolysis-Targeting Chimera (PROTAC) for Targeted Protein Degradation and Cancer Therapy. *J. Hematol. Oncol.* **2020**, *13*, 50.

(7) Jin, Y.; Fan, J.; Wang, R.; Wang, X.; Li, N.; You, Q.; Jiang, Z. Ligation to Scavenging Strategy Enables On-Demand Termination of Targeted Protein Degradation. *J. Am. Chem. Soc.* **2023**, *145*, 7218−7229.

(8) Ishida, T.; Ciulli, A. E3 Ligase Ligands for PROTACs: How They Were Found and How to Discover New Ones. *SLAS Discovery* **2021**, *26*, 484−502.

(9) Luh, L. M.; Scheib, U.; Juenemann, K.; Wortmann, L.; Brands, M.; Cromm, P. M. Prey for the Proteasome: Targeted Protein Degradation-A Medicinal Chemist's Perspective. *Angew. Chem., Int. Ed. Engl.* **2020**, *59*, 15448−15466.

(10) Pettersson, M.; Crews, C. M. Proteolysis TArgeting Chimeras (PROTACs) - Past, Present and Future. *Drug Discov. Today Technol.* **2019**, *31*, 15−27.

(11) Liu, J.; Chen, H.; Liu, Y.; Shen, Y.; Meng, F.; Kaniskan, H.; Jin, J.; Wei, W. Cancer Selective Target Degradation by Folate-Caged PROTACs. *Chem. Soc.* **2021**, *143*, 7380−7387.

(12) He, Q.; Zhou, L.; Yu, D.; Zhu, R.; Chen, Y.; Song, M.; Liu, X.; Liao, Y.; Ding, T.; Fan, W.; Yu, W. Near-Infrared-Activatable PROTAC Nanocages for Controllable Target Protein Degradation and On-Demand Antitumor Therapy. *J. Med. Chem.* **2023**, *66*, 10458−10472.

(13) Miao, Y.; Gao, Q.; Mao, M.; Zhang, C.; Yang, L.; Yang, Y.; Han, D. Bispecific Aptamer Chimeras Enable Targeted Protein Degradation on Cell Membranes. *Angew. Chem., Int. Ed. Engl.* **2021**, *60*, 11267−11271.

(14) Yang, F.; Luo, Q.; Wang, Y.; Liang, H.; Wang, Y.; Hou, Z.; Wan, C.; Wang, Y.; Liu, Z.; Ye, Y.; Zhu, L.; Wu, J.; Yin, F.; Li, Z. Targeted Biomolecule Regulation Platform: A Split-and-Mix PROTAC Approach. *J. Am. Chem. Soc.* **2023**, *145*, 7879−7887.

(15) Song, C.; Jiao, Z.; Hou, Z.; Wang, R.; Lian, C.; Xing, Y.; Luo, Q.; An, Y.; Yang, F.; Wang, Y.; Sha, X.; Ruan, Z.; Ye, Y.; Liu, Z.; Li, Z.; Yin, F. Selective Protein of Interest Degradation through the Split-

and-Mix Liposome Proteolysis Targeting Chimera Approach. *J. Am. Chem. Soc.* **2023**, *145*, 21860−21870.
(16) Han, J.; Liu, Y.; Yang, S.; Wu, X.; Li, H.; Wang, Q. MEK Inhibitors for the Treatment of Non-Small Cell Lung Cancer. *J. Hematol. Oncol.* **2021**, *14*, 1.
(17) Li, T.; Stayrook, S. E.; Tsutsui, Y. K.; Zhang, J.; Wang, Y.; Li, H.; Proffitt, A.; Krimmer, S. G.; Ahmed, M.; Belliveau, O.; Walker, I. X.; Mudumbi, K. C.; Suzuki, Y.; Lax, I.; Alvarado, D.; Lemmon, M. A.; Schlessinger, J.; Klein, D. E. Structural Basis for Ligand Reception by Anaplastic Lymphoma Kinase. *Nature* **2021**, *600*, 148−152.
(18) Akinleye, A.; Furqan, M.; Mukhi, N.; Ravella, P.; Liu, D. MEK and the Inhibitors: from Bench to Bedside. *J. Hematol. Oncol.* **2013**, *6*, 27−11.
(19) Hallberg, B.; Palmer, R. H. The Role of the ALK Receptor in Cancer Biology. *Ann. Oncol.* **2016**, *27*, iii4−iii15.
(20) Zhao, Y.; Adjei, A. The Clinical Development of MEK Inhibitors. *Nat. Rev. Clin. Oncol.* **2014**, *11*, 385−400.
(21) Henderson, Y. C.; Chen, Y.; Frederick, M. J.; Lai, S.; Clayman, G. L. MEK Inhibitor PD0325901 Significantly Reduces the Growth of Papillary Thyroid Carcinoma Cells in vitro and in vivo. *Mol. Cancer Ther.* **2010**, *9*, 1968−1976.
(22) Chen, Y.; Tandon, I.; Heelan, W.; Wang, Y.; Tang, W.; Hu, Q. Proteolysis-Targeting Chimera (PROTAC) Delivery System: Advancing Protein Degraders Towards Clinical Translation. *Chem. Soc. Rev.* **2022**, *51*, 5330−5350.
(23) Ciuffreda, L.; Del Bufalo, D.; Desideri, M.; Di Sanza, C.; Stoppacciaro, A.; Ricciardi, M. R.; Chiaretti, S.; Tavolaro, S.; Benassi, B.; Bellacosa, A.; Foà, R.; Tafuri, A.; Cognetti, F.; Anichini, A.; Zupi, G.; Milella, M. Growth-Inhibitory and Antiangiogenic Activity of the Mek Inhibitor PD0325901 in Malignant Melanoma with or without BRAF Mutations. *Neoplasia* **2009**, *11*, 720−W6.
(24) Packer, L. M.; East, P.; Reis-Filho, J. S.; Marais, R. Identification of Direct Transcriptional Targets of (V600E) BRAF/MEK Signalling in Melanoma. *Pigm. Cell Melanoma Res.* **2009**, *22*, 785−798.
(25) Wei, J.; Hu, J.; Wang, L.; Xie, L.; Jin, M. S.; Chen, X.; Liu, J.; Jin, J. Discovery of a First-in-Class Mitogen-Activated Protein Kinase Kinase 1/2 Degrader. *J. Med. Chem.* **2019**, *62*, 10897−10911.
(26) Hao, Z.; Ren, L.; Zhang, Z.; Yang, Z.; Wu, S.; Liu, G.; Cheng, B.; Wu, J.; Xia, J. A Multifunctional Neuromodulation Platform Utilizing Schwann Cell-Derived Exosomes Orchestrates Bone Microenvironment via Immunomodulation, Angiogenesis and Osteogenesis. *Bioact. Mater.* **2023**, *23*, 206−222.
(27) Wang, Z.; An, J.; Zhu, D.; Chen, H.; Lin, A.; Kang, J.; Liu, W.; Kang, X. Periostin: an Emerging Activator of Multiple Signaling Pathways. *J. Cell Commun. Signal.* **2022**, *16*, 515−530.
(28) He, Y.; Sun, M.; Zhang, G.; Yang, J.; Chen, K.; Xu, W.; Li, B. Targeting PI3K/Akt Signal Transduction for Cancer Therapy. *Signal Transduction Targeted Ther.* **2021**, *6*, 425.
(29) Liu, R.; Chen, Y.; Liu, G.; Li, C.; Song, Y.; Cao, Z.; Li, W..; Hu, J.; Lu, C.; Liu, Y. PI3K/AKT Pathway as a Key Link Modulates the Multidrug Resistance of Cancers. *Cell Death Dis.* **2020**, *11*, 797.
(30) Chong, C. R.; Jänne, P. A.; Pasi, A.; Jänne. The Quest to Overcome Resistance to EGFR-Targeted Therapies in Cancer. *Nat. Med.* **2013**, *19*, 1389−1400.
(31) He, Z.; He, J.; Xie, K. KLF4 Transcription Factor in Tumorigenesis. *Cell Death Discovery* **2023**, *9*, 118.
(32) Lu, J.; Guan, H.; Wu, D.; Hu, Z.; Zhang, H.; Jiang, H.; Yu, J.; Zeng, K.; Li, H.; Zhang, H.; Pan, C.; Cai, D. Yu X.; et al. Pseudolaric acid B ameliorates synovial inflammation and vessel formation by stabilizing PPARγ to inhibit NF-κB signalling pathway. *J. Cell. Mol. Med.* **2021**, *25*, 6664−6678.
(33) Cao, C.; He, M.; Wang, L.; He, Y.; Rao, Y. Chemistries of Bifunctional PROTAC Degraders. *Chem. Soc. Rev.* **2022**, *51*, 7066−7114.

https://doi.org/10.1021/jacsau.4c00278
JACS Au 2024, 4, 2915−2924